Petroleum Science 21 (2024) 1508–1523

Contents lists available at ScienceDirect

Petroleum Science

journal homepage: www.keaipublishing.com/en/journals/petroleum-science

Original Paper

Further study on the genesis of lamellar calcite veins in lacustrine black shale—A case study of Paleogene in Dongying Depression, China

Guan-Min Wang*, Yun-Jiao Zhang, Zi-Yuan Yin, Rui Zhu, Zhi-Yao Hou, Yu Bai

School of Geosciences, China University of Petroleum (East China), Qingdao, 266580, Shandong, China

ARTICLE INFO

Article history:
Received 1 April 2023
Received in revised form
1 August 2023
Accepted 27 December 2023
Available online 30 December 2023

Edited by Jie Hao and Meng-Jiao Zhou

Keywords:
Calcite veins
Shale diagenesis
Material source
Formation period
Formation mechanism

ABSTRACT

Lamellar calcite veins are prevalent in carbonate-rich, lacustrine dark shale. The formation mechanisms of these veins have been extensively debated, focusing on factors such as timing, depth, material source, and driving forces. This paper examines dark lacustrine shale lamellar calcite veins in the Paleogene strata of Dongying Depression, using various analytical techniques: petrography, isotope geochemistry, cathodoluminescence, inclusion thermometry, and electron probe micro-analysis. Two distinct types of calcite veins have been identified: granular calcite veins and sparry calcite veins. These two types differ significantly in color, grain structure, morphology, and inclusions. Through further investigation, it was observed that vein generation occurred from the shallow burial period to the maturation of organic matter, with a transition from granular calcite veins to sparry calcite veins. The granular calcite veins exhibit characteristics associated with the shallow burial period, including plastically deformed laminae and veins, the development of strawberry pyrite, the absence of oil and gas, weak fractionation in oxygen isotopes, and their contact relationship with sparry calcite veins. These granular calcite veins were likely influenced by the reduction of sulfate bacteria. On the other hand, sparry calcite veins with fibrous grains are antitaxial and closely linked to the evolution and maturation of organic matter. They contain oil and gas inclusions and show a distribution range of homogenization temperature between 90 °C and 120 °C and strong fractionation in oxygen isotopes, indicating formation during the hydrocarbon expulsion period. The carbon isotope analysis of the surrounding rocks and veins suggests that the material for vein formation originates from the shale itself, specifically authigenic micritic calcite modified by the action of methanogens. The opening of horizontal fractures and vein formation is likely driven by fluid overpressure resulting from undercompaction and hydrocarbon expulsion. Veins may form rapidly or through multi-stage composite processes. Early veins are predominantly formed in situ, while late veins are a result of continuous fluid migration and convergence. Furthermore, the veins continue to undergo modification even after formation. This study emphasizes that the formation of lamellar calcite veins in shale is a complex diagenetic process influenced by multiple factors: biology, organic matter, and inorganic processes, all operating at various stages throughout the shale's diagenetic history.

1. Introduction

In sedimentary basins worldwide, particularly in lacustrine or marine sedimentary basins in China, calcite veins frequently develop parallel to laminae in carbonate-rich black shale (Rodrigues et al., 2009; Cobbold et al., 2013; Zhao et al., 2014; Yu et al., 2015; Tribovillard et al., 2018; Luan et al., 2019; Ma et al., 2020; Wu et al., 2021). These calcite veins contain valuable information related to diagenetic fluid properties, organic matter, and the diagenetic evolution of shale minerals. Studying the genesis of lamellar calcite veins allows for the tracing of the interaction process between organic and inorganic diagenetic evolution in shales (Liang et al., 2018; Tribovillard et al., 2018; Li et al., 2020; Wu et al., 2021). Moreover, these veins serve as a proxy for evaluating shale reservoirs (Liu et al., 2019; Zhang et al., 2021). At the beginning of 2020, a significant milestone was achieved in China's continental fault basin as shale oil exploration in the Niuzhuang sag of Dongying depression resulted in a breakthrough. One well in this area recorded a daily output exceeding 100 t. By February 2022, the

* Corresponding author.
E-mail address: wangguanmin@upc.edu.cn (G.-M. Wang).

https://doi.org/10.1016/j.petsci.2023.12.022

production peak of shale oil in the FY 1-1HF well reached an impressive 262.8 t/d. Exploration efforts revealed a distinctive characteristic of the key reservoir for shale oil in the lower Es_3—upper Es_4 formations in Dongying Depression. The crucial factor here is the presence of interlayer fractures associated with lamellar sparry calcite veins (refer to Fig. 1). This distinguishing feature sets it apart from shale oil and gas reservoirs found in other basins.

Based on the direction of crystal growth and the location of crystal growth within developing veins, fibrous grain veins, such as calcite and gypsum, can be classified as syntaxial, ataxial, or antitaxial veins (Durney and Ramsay, 1973; Oliver and Bons, 2001; Bons et al., 2012). Antitaxial calcite veins have parallel boundaries, and fibrous grains grow from the median zone (Bons et al., 2012) towards the two boundaries of the surrounding rocks. This growth pattern resembles the muscle fiber of an animal, earning it the nickname 'Beef' (Lang et al., 1923; Durney and Ramsay, 1973; Bons and Montenari, 2005). These veins have been a subject of significant interest among researchers and are also a focus of this paper. Additionally, there are recrystallized grain calcite veins found in the lacustrine dark shale of Dongying Depression. Despite receiving limited attention, some studies mention them as the median zone of fibrous veins (Luan et al., 2019; Teng et al., 2020). However, this study reveals that these veins often exist independently and that their development reflects the diagenetic evolution process of shale.

The formation mechanisms of lamellar calcite veins have been the subject of extensive debate, focusing on various aspects such as the timing and burial depth of vein generation, the source of vein material, driving forces for vein initiation and widening, and the growth direction and mechanism. Scholars generally agree that the material source for vein formation is the authigenic micritic calcite present in the shale surrounding the veins, rather than coming from an external source (Rodrigues, 2008; Rodrigues et al., 2009; Yu et al., 2015; Meng et al., 2017; Tribovillard et al., 2018; Luan et al., 2019; Su et al., 2022). Lamellar calcite veins are commonly found in mature source rocks, and their formation is often attributed to hydrocarbon generation and expulsion during the thermal evolution of source rocks (Stoneley, 1983; Rodrigues et al., 2009; Cobbold et al., 2013; Zanella et al., 2014; Zhang et al., 2016; Wu et al., 2021). In a study of calcite veins in the Argentina Neuquén Basin, Larmier et al. (2021) found a positive correlation between the maturity of source rocks and the number and density of veins. Fluid overpressure is considered a critical factor in forming horizontal micro-cracks. Fluid seepage force counters the rock's weight, generating effective tensile stress, which leads to the development of horizontal fracturing cracks in shale (Cobbold and Rodrigues, 2007). The thermal evolution of organic matter, especially hydrocarbon expulsion, plays a vital role in overpressure formation (Oliver and Bons, 2001; Ma et al., 2016; Zhang et al., 2016). Wang et al. (2020) reconstructed the trapping pressure of hydrocarbon inclusions in veins and found that the process of hydrocarbon generation and expulsion can lead to fluid overpressure close to or exceeding the lithostatic pressure, thereby promoting the formation of horizontal fractures and veins. Recently, Wang et al. (2023) discovered that asymmetric veins on both sides of the median zone reflect episodic hydrocarbon expulsion from source rocks and the initial migration of oil and gas. Geochemical indicators suggest that the veins have undergone multiple stages, with each stage reflecting a hydrocarbon expulsion process. Additionally, the dehydration of clay or gypsum and the crystallization force of crystal growth have been proposed as explanations for the formation of calcite veins (Means and Li, 2001; Bolås et al., 2004; Lahann and Swarbrick, 2011; Wang et al., 2018a; Luan et al., 2019).

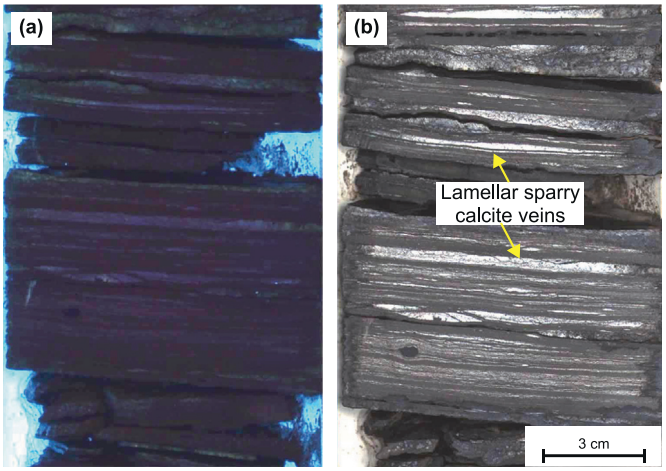

Fig. 1. Macroscopic characteristics of lamellar sparry calcite veins in core: **(a)** fluorescent photograph; **(b)** core photograph. Well N55-X1, 3493.4 m.

Indeed, the formation of lamellar calcite veins can be influenced by various factors beyond hydrocarbon generation and expulsion. Research conducted in different regions highlights the role of other controlling factors in the formation of these veins. In the Paris Basin, Zanella et al. (2021) emphasized the significance of compressional tectonic stress in the formation of fractures. They found that calcite veins often developed during periods of basin horizon shortening, and through U/Pb dating, they determined the period to be 155 ± 19 Ma. Similarly, in other basins, such as the Magallanes Basin in Chile and Argentina, the Wessex Basin in the UK, and the Neuquén Basin in Argentina, calcite veins have also been associated with compressive tectonic stress (Zanella et al., 2014, 2015a, 2015b; Ukar et al., 2017, 2020). Furthermore, the action of bacteria during the shallow burial period is considered to play a role in the formation of calcite veins, particularly involving sulfate-reducing bacteria (Al-Aasm et al., 1993, 1995; Yu et al., 2015; Meng et al., 2017; Tribovillard et al., 2018). Microbially driven sulfate reduction can contribute to calcite saturation (Gallagher et al., 2014). Petrographic observations of veins provide supporting evidence, such as plastic deformation of shale and veins, the presence of pyrite, and authigenic albites in veins (Maher et al., 2017; Meng et al., 2018, 2019; Hrabovszki et al., 2020). Recently, Su et al. (2022) conducted U/Pb dating of calcite veins in the Nanxiang Basin, China, and determined an age of 41.02 ± 0.44 Ma. Their findings indicated that calcite veins were early diagenetic products formed before the complete compaction and consolidation of shale, with a formation depth ranging between 500 m and 800 m. All these research findings highlight the complexity of factors influencing the formation of lamellar calcite veins and emphasize the need to consider multiple mechanisms when studying these geological features.

The formation mechanism of calcite veins has been a subject of research. In syntaxial veins, crystals experience stretching due to the repeated addition of vein material in successive crack-seal events (Ramsay, 1980). This crack-seal mechanism provides an

explanation for the formation of fibrous calcite veins. However, antitaxial calcite veins pose a challenge to the crack-seal mechanism, as the fibrous grains in these veins grow continuously without obvious growth competition (Bons and Montenari, 2005; Wang et al., 2020; Su et al., 2022). Wang et al. (2020) argued that vein dilation in the absence of lithostatic fluid pressure suggests a primarily steady-state process, where dilation is accommodated and offset by narrowing of the adjacent wall-rock laminae (Meng et al., 2018). Means and Li (2001) proposed that the fiber tips remain in contact with the wall rock rather than growing into a crack. Additionally, a fluid film (Su et al., 2022) is present at the contact, allowing the vein to act as a permeable conduit for horizontal advection, which can influence the formation of displacive veins (Wang et al., 2023). Subvertical fibers can actively displace the wall rock against the vertical overburden load, leading to the formation of displacive veins (Meng et al., 2018; Hrabovszki et al., 2020; Su et al., 2022).

In this study, the researchers build upon previous studies to investigate the lamellar calcite veins found in the black lacustrine shale of the upper Es_4–lower Es_3 formations in the Paleogene strata of Dongying Depression. We employ various analytical techniques, including microscopic observation, cathodoluminescence (CL), inclusion thermometry (IT), electron probe micro-analysis (EPMA), and carbon and oxygen isotope tests (C–O IT), to further analyze the material source, formation period, and crystallization process of these calcite veins.

2. Geological setting

Dongying Depression is situated in the southeastern part of the Jiyang Depression within the Bohai Bay basin in China. It is characterized as a Mesozoic and Cenozoic dustpan fault-depressed lake basin that has developed on the Paleozoic basement (Yu et al., 2022a). The depression spans a length of approximately 90 km and has a width of around 65 km, covering an area of 5700 km^2. It can be subdivided into four negative secondary structures and three positive secondary structures, including the Niuzhuang Sag, Minfeng Sag, Lijin Sag, and Boxing Sag. Additionally, there is a northern fault terrace belt (Binxian and Chenjiazhuang Salient), a central anticline, and a southern gentle slope belt (Luxi Uplift and Guangrao Salient) (Fig. 2(a), (b)). The depression's strata consist of the Kongdian Formation, Shahejie Formation, Dongying Formation, Guantao Formation, Minghuazhen Formation, and Pingyuan Formation, arranged from the bottom to the top of the geological sequence. The sedimentary thickness in the depression exceeds 3500 m (Fig. 3) (Wu et al., 2018; Peng et al., 2020).

During the sedimentary period from the upper Es_4 to the lower Es_3, the climate in the study area experienced a gradual transition from drought to humid conditions. The continued subsidence of the basement led to an increase in the accommodating space of the lake basin, transforming it into semi-deep and deep lacustrine facies (Pang et al., 2019). This geological setting resulted in the deposition of a substantial thickness of lacustrine black shale in the central area of the lake basin. Being the main source rocks in the depression, these black shales provided favorable conditions for hydrocarbon generation (Chen et al., 2018; Li et al., 2019). The shale in this region primarily comprises felsic, carbonate, and clay minerals, with well-developed laminae (Wang et al., 2018b; Pang et al., 2019). Sparry calcite veins, characterized by fibrous grains that run parallel to the laminae, are widespread in the area and show a clear correlation with the black shale (Wang et al., 2005; Luan et al., 2019; Teng, 2020). This paper focuses on studying the lamellar calcite veins found in the upper Es_4 to lower Es_3 formations within the Niuzhuang Sag of the Dongying Depression, conducting related research to explore their origin and significance.

3. Samples and methodology

In this research, shale samples were collected from several wells in the study area, including N55-X1, NX55, NY1, and FY1. The collected samples were prepared for analysis, and their lithofacies were observed under the DM2700P polarizing microscope. For the experimental part of the study, samples were taken specifically from well N55-X1, with burial depths ranging from 3334.05 m to 3609.5 m. The composition and total organic carbon (TOC) content of these samples were analyzed to understand their mineral and organic composition. A total of 124 samples were used for carbon and oxygen isotope testing (C–O IT), 12 samples for inclusion thermometry (IT), and 17 samples for cathodoluminescence (CL) and electron probe micro-analysis (EPMA) (Fig. 4).

In the research, cathodoluminescence (CL) experiments were conducted on polished sections using the CLF-2 cathodoluminescence system at 15 kV and 300 mA. The purpose of these experiments was to identify the growth stages of the veins, providing insights into their diagenetic history. To measure the homogenization temperature (Th) of two-phase inclusions in sparry calcite veins, an INSTEC mK2000 heating-freezing stage was used. The temperature measurement of inclusions followed the oil and gas industry standard of the People's Republic of China (SY/T6010-94). The inclusion to be measured was located using a microscope, and the heating rate was controlled at 3 °C/min to 10 °C/min. When the inclusion approached its Th, the heating rate was adjusted to 1 °C/min. Three measurements were taken for each inclusion to obtain an average value.

The carbon and oxygen isotopes of calcite veins and the surrounding rocks were also analyzed. The testing process involved first extracting in situ calcite samples using a small micro-drill. The calcite was then separated and purified to achieve a purity of more than 99%. The sample was ground to 200 mesh before conducting the standard phosphoric acid method test to determine the carbon and oxygen isotope values. Additionally, electron probe micro-analysis (EPMA) was employed to analyze the micro-area elements of the lamellar calcite veins. Using the JXA-8230 electron probe microscope under the conditions of 15 kV and 1×10^{-8} A, samples were tested to quantitatively study the micro-area element content, providing valuable information about the composition of the veins. These analytical techniques were used to gain a comprehensive understanding of the calcite veins and their geological context, shedding light on their formation, evolution, and significance within the study area.

4. Results

4.1. Characteristics of microscopic petrography

In the lacustrine dark shale of the upper Es_4–lower Es_3, the core samples reveal that calcite veins are predominantly distributed parallel to the laminae in the shale. Additionally, isolated calcite veins can be observed, often appearing in a lenticular shape. Some veins exhibit folding and deformation, interacting with the surrounding shale laminae (Fig. 5(a), (b)). The density of the laminae in the shale is positively correlated with the development of calcite veins. In the areas where the veins are well-developed, the surrounding rock laminae are typically a combination of organic-rich

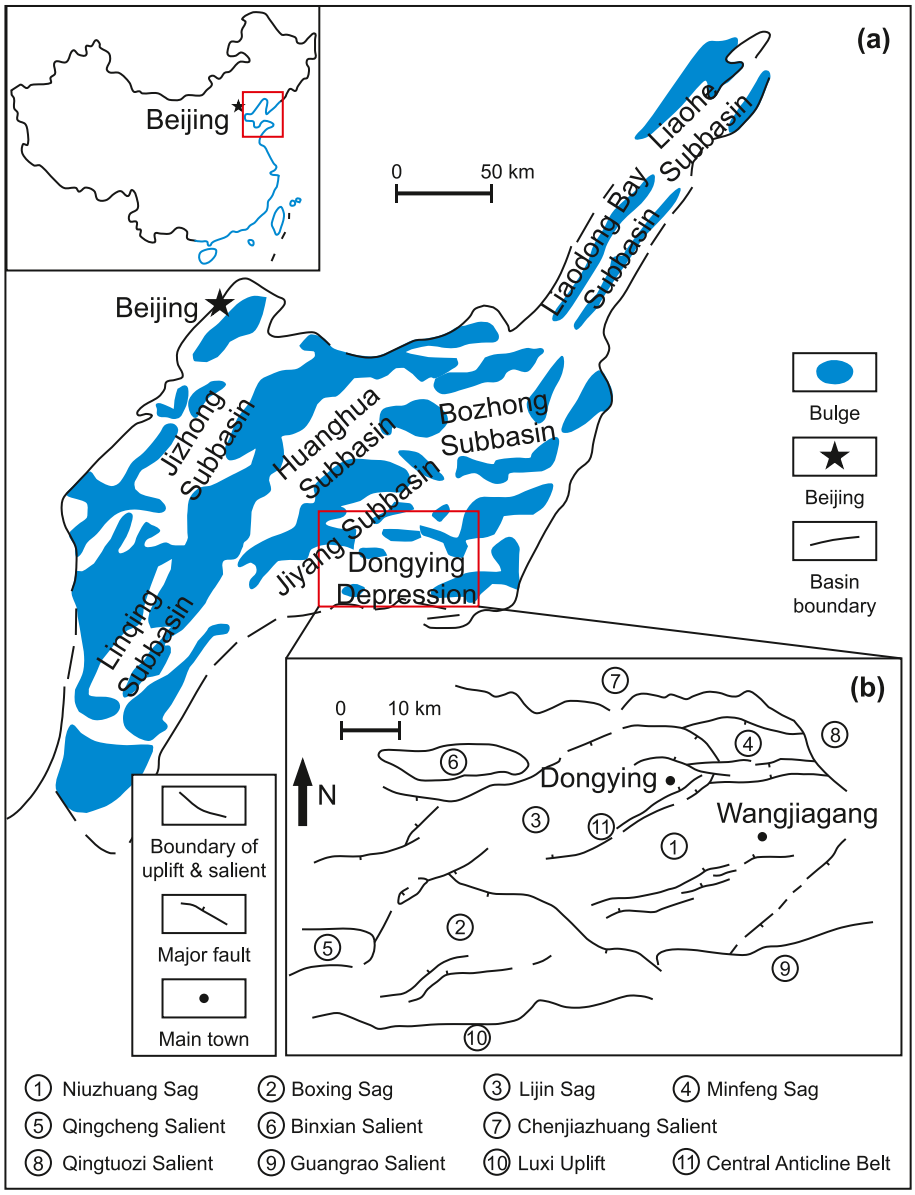

Fig. 2. Map of study area (modified according to reference Luan et al., 2019). **(a)** Tectonic units of Bohai Bay Basin and regional position of Dongying Depression. **(b)** Tectonic units of Dongying Depression.

and carbonate-rich laminae. Two distinct types of calcite veins can be identified in thin sections based on their color, shape, grain size, and special composition (Fig. 5(c), (d)). The first type is a granular calcite vein, characterized by a grayish-yellow color. These veins often appear as isolated lenticular and thin laminae. The grains in these veins range from powder to fine grains, and dispersed crystalline pyrite particles with a size of more than 10 μm can be observed inside the veins. This type of vein frequently shows signs of folding and deformation (Fig. 5(g)). The second type is the sparry calcite vein, which predominantly develops parallel to the shale bedding, resembling the shale laminae. Some of these veins grow and develop along the edge of the granular calcite veins, forming a combination of the two vein types. Within sparry calcite veins, structures like 'BEEF' and 'CONE IN CONE' can be found (Cobbold et al., 2013) (Fig. 5(e), (f)). The particles in these veins appear clean and bright, with a thicker size. The morphological characteristics of the thick particles are fibrous, and their growth direction is perpendicular to the surrounding rock's thin layers. In some veins, a median zone is present. When observed under orthogonal light, the crystals on both sides of the median zone show the same optical characteristics (Fig. 5(h)), indicating that the mineral veins' growth may possess antitaxial development attributes (Durney and Ramsay, 1973; Wang et al., 2018a; Zhao et al., 2020). It's worth noting that solid parcels in the surrounding rocks are also observed to be retained during the growth of these mineral veins.

On vertical slices, the kerogen present in the shale exhibits yellow fluorescence, while the oil and gas display blue fluorescence. In the lenticular calcite vein, the gray-yellow granular calcite does not exhibit any fluorescence, whereas the sparry calcite shows weak blue fluorescence (Fig. 6(a), (b)). These characteristics are also observed in lamellar calcite veins. The granular calcite veins and

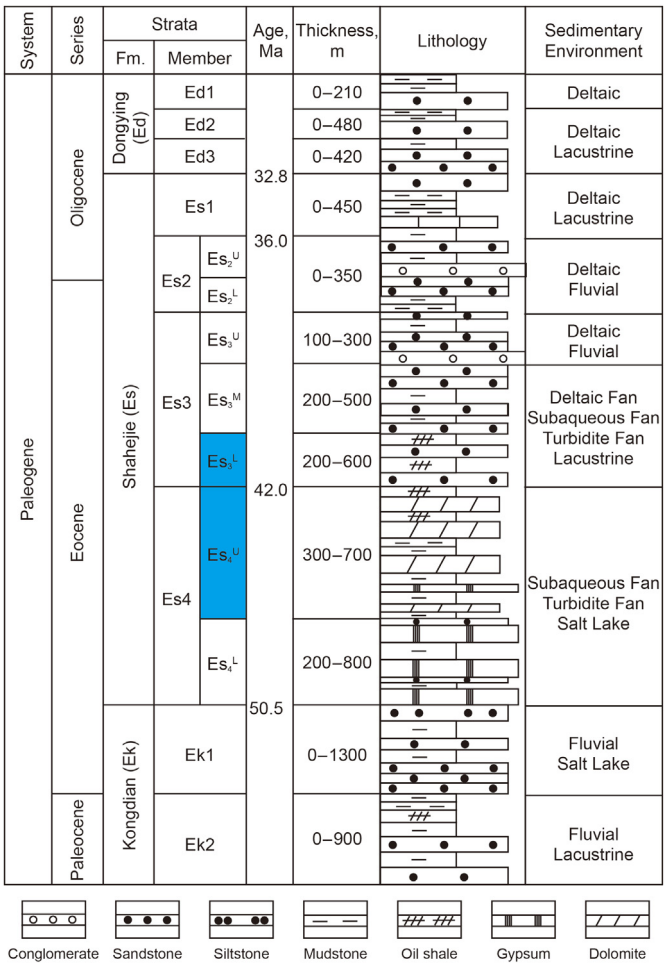

Fig. 3. Paleogene sedimentary strata in Dongying Depression (modified according to reference Luan et al., 2019).

granular calcite as the median zone show no fluorescence, but the sparry calcite exhibits blue fluorescence (Fig. 6(c), (d)).

On horizontal slices, the sparry calcite veins display a blue-white fluorescence mainly in intergranular spaces and microcracks, extending along the direction of these cracks (Fig. 6(e), (f)). The fluorescence characteristics indicate that the sparry calcite veins are closely associated with the migration of oil and gas. It suggests that the development space of sparry calcite veins served as a channel for oil and gas migration.

Through cathodoluminescence (CL) observation, significant color differences can be observed between granular calcite and sparry calcite (Fig. 7(a)–(d)). Granular calcite veins are often squeezed on one side by sparry calcite veins or clamped in the middle, resulting in thick calcite veins formed by multi-stage recombination. The varying CL colors of veins formed in different periods suggest that the fluid components during their crystallization were different (Fig. 7(d)). In some thick veins, the CL colors display alternating bright red and dark red bands, indicating that the laminae ruptured along the edge of the early veins after their formation. Subsequently, other fluids entered and recrystallized to form a new vein, combined with the early vein to create a new thick vein. Inside these thick veins, late healing cracks that truncate interactively can also be observed. The CL color of the healing cracks is significantly different from that of the vein, indicating that the later fluid entered the earlier vein's fracture under pressure, leading to calcite crystallization (Fig. 7(e), (f)). In contrast, the color of the cathodoluminescence in single thin-layer calcite veins is generally relatively consistent, indicating that the formation of these single thin-layer calcite veins occurred in a single stage.

4.2. Characteristics of inclusion petrography

In the sparry calcite veins, various types of inclusions have been identified, including solid bitumen inclusions, two-phase hydrocarbon inclusions, and a small number of brine inclusions. These inclusions exhibit different shapes, such as elliptical, rectangular, and irregular shapes. On horizontal slices, hydrocarbon inclusions are predominantly observed in a beaded or banded pattern, distributed around the intercrystalline or intercrystalline healing cracks. These inclusions exhibit blue-white fluorescence when viewed under the microscope. On vertical slices, it is apparent that the distribution of hydrocarbon inclusions is consistent with the growth direction of fibrous calcite crystals. They show a banded arrangement perpendicular to the direction of the surrounding rock (Fig. 8(a)–(d)).

The two-phase hydrocarbon inclusions thermometry results indicate that the homogenization temperature (Th) of the majority of inclusions is concentrated within the range of 90–120 °C. This temperature range corresponds to the hydrocarbon expulsion period, suggesting that the formation of these calcite veins occurred during this specific geological stage when hydrocarbons were actively migrating. In addition to the hydrocarbon inclusions, a small number of two-phase brine water inclusions were also isolated in the calcite veins. The measured Th forese brine inclusions can reach higher temperatures, specifically within the range of 140–150 °C. This observation indicates that the calcite veins underwent reformation by fluid during the late stage of significant oil and gas migration. These veins continued to crystallize and undergo modifications during this later phase (Fig. 9).

4.3. Geochemical characteristics of stable isotopes

The calcite vein and surrounding rock samples from well N55-X1 were classified based on their grain sizes. Their carbon and oxygen isotope values were analyzed (Table 1). The surrounding rock contains micrite calcite with a $\delta^{13}C_{V\text{-}PDB}$ value ranging from 2.28‰ to 7.91‰, and an average of ~4.13‰. The calcite veins in powder-fine, medium, and coarse grains exhibit $\delta^{13}C_{V\text{-}PDB}$ values ranging from 2.24‰ to 4.90‰ (average 3.72‰), 2.06‰–5.45‰ (average 4.00‰), and 2.52‰–5.99‰ (average 4.77‰), respectively. The variation range of $\delta^{13}C_{V\text{-}PDB}$ values in calcite veins of different grain sizes is relatively close, centered around 4‰ (Fig. 10). Regarding the $\delta^{18}O_{V\text{-}PDB}$ values, significant differences are observed among the four types of calcite. The micrite calcite in the surrounding rock exhibits $\delta^{18}O_{V\text{-}PDB}$ values ranging from −9.89‰ to −2.45‰, with an average of −7.82‰. The $\delta^{18}O_{V\text{-}PDB}$ values of powder-fine, medium, and coarse-grained calcite veins range from −12.97‰ to −7.33‰ (average −9.29‰), −14.12‰ to −9.42‰ (average −11.66‰), and −13.29‰ to −8.20‰ (average −11.38‰), respectively. As the grain size increases, the $\delta^{18}O_{V\text{-}PDB}$ values become more negative, especially for the medium and coarse grain calcite veins, with an average $\delta^{18}O_{V\text{-}PDB}$ value of about −11‰ (Fig. 10). These differences in carbon and oxygen isotopes among the different calcite samples are closely related to the material source and diagenetic evolution of the calcite veins.

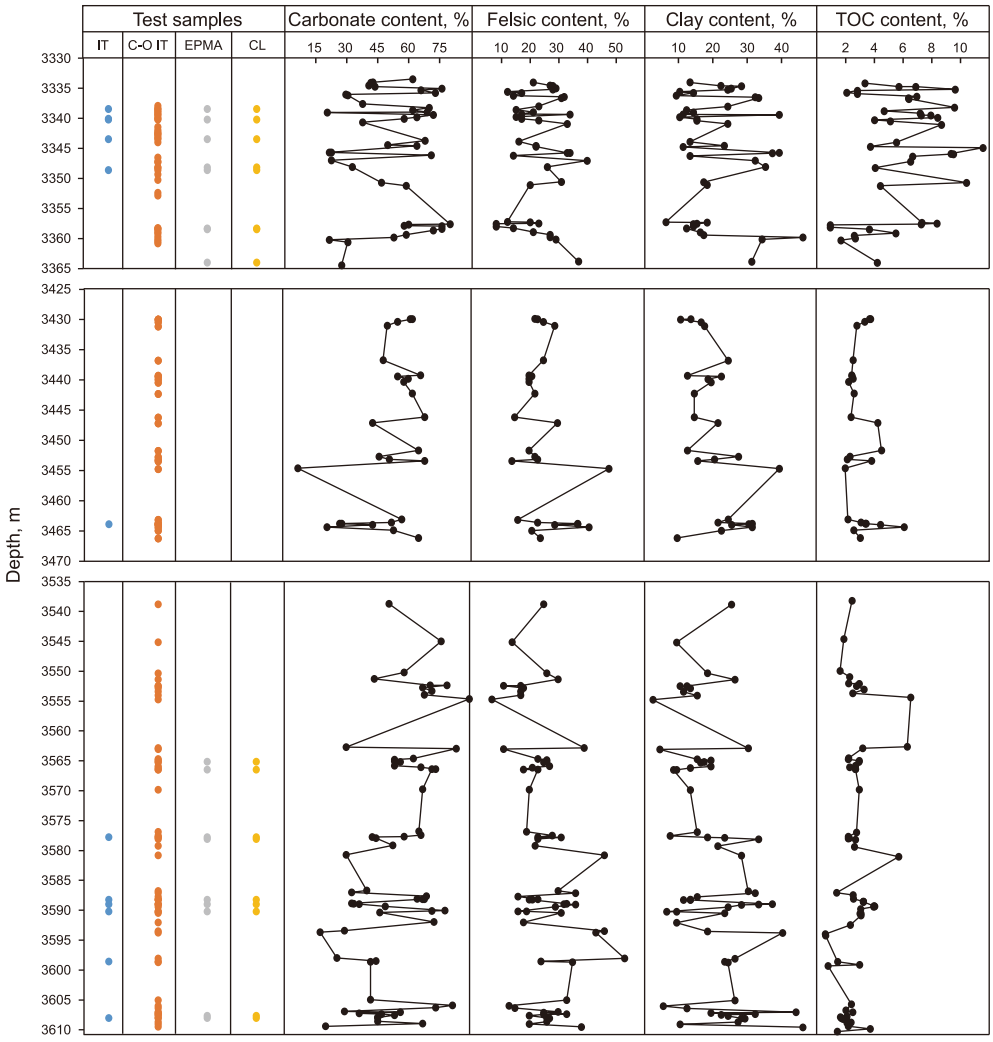

Fig. 4. Burial depth, composition, TOC content of samples and experimental items in Well N55-X1.

4.4. Element analysis of electron probe

In the electron probe element analysis of the 17 samples and 50 different types of veins, a total of 129 data points were tested to obtain the content of chemical components in the various veins (Table 2). The results show that granular calcite veins have higher SiO_2 and Al_2O_3 content and lower MnO content, indicating the presence of certain clay minerals in these veins. On the other hand, sparry calcite veins have lower SiO_2 and Al_2O_3 contents and higher MnO content. Apart from SiO_2, Al_2O_3, and MnO, there were no significant differences in the contents of other chemical components among the veins.

The lamellar sparry calcite vein with an obvious median zone is selected, and the sampling test is carried out in the direction from the one side edge to the median zone, then to another side edge. The results show that the content of FeO is high near the median zone of the vein, which changes a little in other parts. The higher FeO content is related to the residual clay minerals in the median zone. The MnO content varies symmetrically along the median zone and gradually increases to both sides, which is consistent with the CL characteristic that calcite veins show a gradual transition from dark red to bright red. This feature shows that the crystallization of thick calcite veins is a long-term continuous process. During this process, the content of Mn ion provided by the fluid keeps increasing (Fig. 11).

5. Discussion

5.1. Material source for formation of lamellar calcite veins

In this study, the stable carbon isotopes in different carbon pools were used to track the carbon sources involved in the carbonate dissolution and recrystallization process (Cao et al., 2018). Organic matter can provide CO_2 rich in ^{12}C and lead to the ^{13}C ranges from −33‰ to −18‰ and the ^{13}C value of inorganic carbon in the atmosphere is about −7‰ (Mack et al., 1991). Sulfate bacteria can reduce organic matter and generate CO_2 ($\delta^{13}C_{V\text{-}PDB} \approx -25‰$), and methanogen bacteria can also provide CO_2 which ^{13}C is higher to 15‰ (Irwin et al., 1977; Raiswell, 1987; Wolff et al., 1992).

The main material source of calcite vein formation in the shale was found to be argillaceous calcite, which was precipitated in the early stage of the lake. These calcites were later modified by the

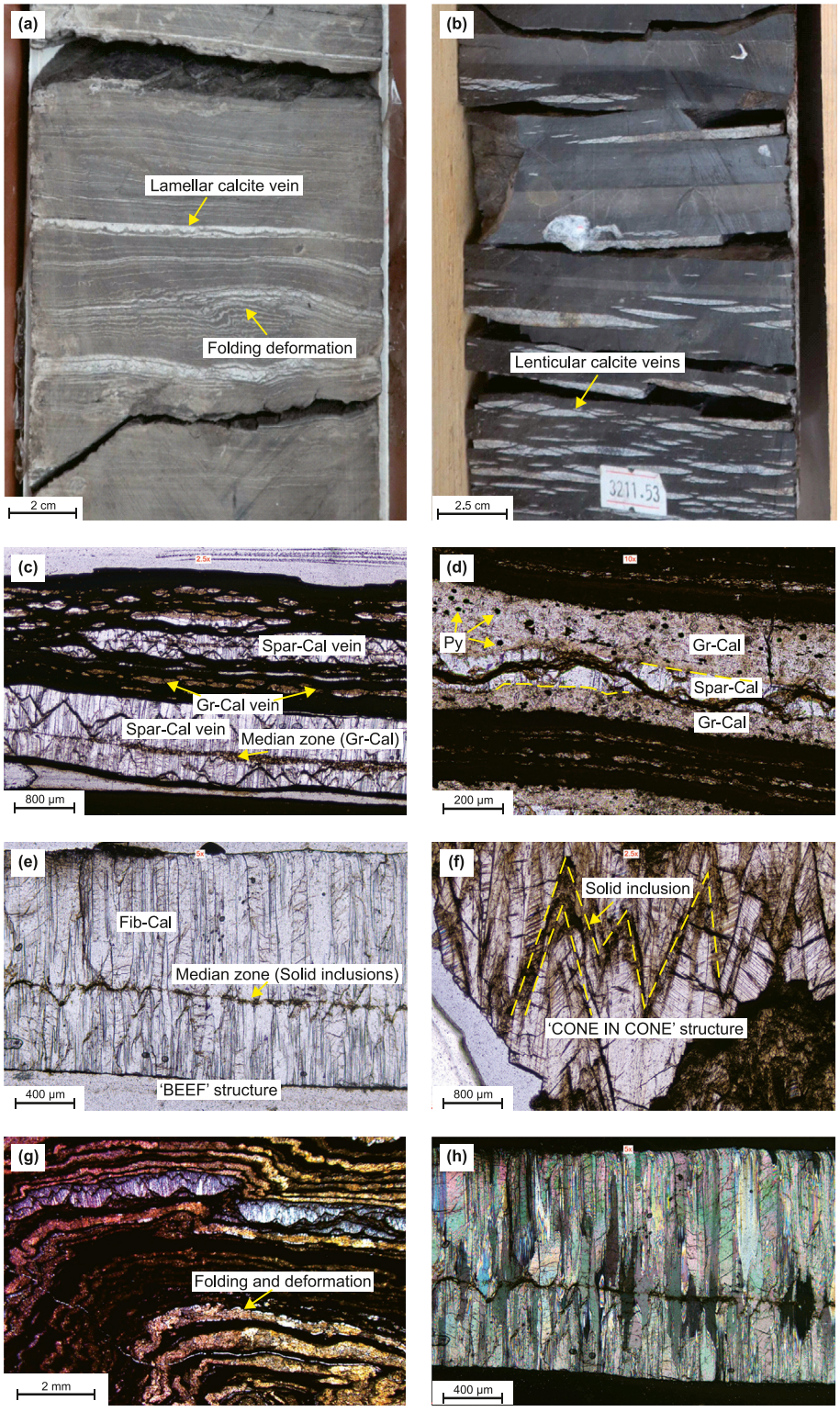

Fig. 5. Microscopic petrographic characteristics of calcite veins Granular calcite (Gr-Cal), Sparry calcite (Spar-Cal), Fibrous calcite (Fib-Cal), Pyrite (Py). **(a)** Lamellar calcite veins are distributed along the laminae direction in shale, and some veins are folded and deformed with shale laminae. Well NX55, 3783.55 m. **(b)** Spar-Cal veins in lenticular accumulate in shale laminae while hardly developing in the massive structural shale. Well FY1, 3211.53 m. **(c)** Gr-Cal veins in lenticular and lamellar Spar-Cal veins develop in shales. The median zone of Spar-Cal vein is composed of granular calcite. Well N55-X1, 3340.5 m. **(d)** Spar-Cal veins grow along the edge of Gr-Cal veins, and crystalline pyrite is distributed in Gr-Cal vein. Well N55-X1, 3590.17 m. **(e)** Spar-Cal veins develop 'BEEF' structure with median zone. The median zone consists of solid shale inclusions and Fib-Cal grows on both sides. Well N55-X1, 3345.77 m. **(f)** Spar-Cal veins develop 'CONE IN CONE' structure with solid shale inclusions mixed. Well N55-X1, 3578.03 m. **(g)** Gr-Cal veins in the color of grayish-yellow develop folding and deformation with shale lamina. well NY1, 3437.31 m. **(h)** Fibrous calcites on both sides of the median zone in the lamellar Spar-Cal vein have the same optical properties. Well N55-X1, 3345.77 m.

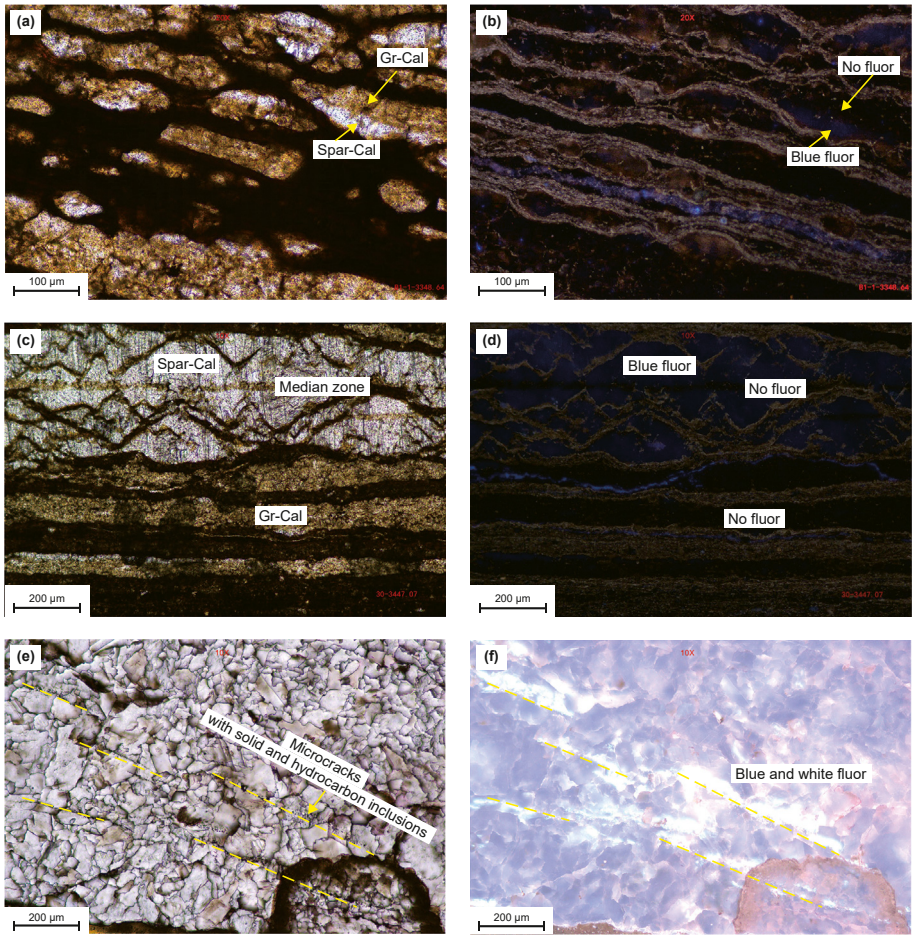

Fig. 6. The fluorescence (fluor) characteristics of different calcite veins. **(a)** Lenticular veins combined with Gr-Cal and Spar-Cal. Well N55-X1, 3358.64 m. **(b)** The figure is a fluorescence image of **(a)**. Under fluorescence, Gr-Cal shows no fluorescence phenomenon, and Spar-Cal has blue fluorescence. **(c)** Spar-Cal vein with median zone and Gr-Cal veins. Well N55-X1, 3447.07 m. **(d)** The figure is a fluorescence image of **(c)**. Blue fluorescence occurs in lamellar Spar-Cal veins, and there is no fluorescence in Gr-Cal vein and median zone composed of Gr-Cal. **(e)** Parallel to the extension direction of veins, there are many healing microcracks in the veins. Well N55-X1, 3590.17 m. **(f)** The figure is a fluorescence image of **(e)**. Hydrocarbon inclusions shows blue-white fluorescence, and solid inclusions are developed at the edge of the microcracks.

biochemical action of methanogens. Methanogens are bacteria that can decompose organic matter in an anoxic environment, producing methane, hydrogen, carbon dioxide, and other substances. During this process, the carbon isotopes can separate. The methane gas produced by methanogens is enriched in the lighter ^{12}C isotope, while the corresponding carbon dioxide gas is enriched in the heavier ^{13}C isotope. These carbon dioxides, rich in heavy ^{13}C isotopes, can be saturated and precipitated in solution to form micrite carbonate minerals with $\delta^{13}C_{V\text{-}PDB}$ values up to 7.91‰ (Cao et al., 2018). After dissolution and recrystallization, the calcite veins still maintain the carbon isotope composition of these micrite carbonate minerals, resulting in little change in the ^{13}C value with the increase of burial depth (Myrttinen et al., 2012; Zhang et al., 2022). The carbon isotope test results in this study show that the ^{13}C isotope values of micrite calcite and different grain sizes of calcite veins are all related to carbonate areas with biogenic gas genesis. The $\delta^{13}C_{V\text{-}PDB}$ of grayish-yellow granular calcite veins is lower than that of sparry calcite veins in medium-coarse grain, which may be related to sulfate bacterial reduction. This is further supported by the presence of pyrite in the granular calcite veins. The formation of sparry calcite veins is mainly due to the dissolution of micrite carbonate formed by methane bacteria in the surrounding rocks and subsequent recrystallization (Fig. 10).

The fractionation of oxygen isotopes during diagenesis is an important process that reflects water-rock interactions and can provide valuable information about the formation temperature and fluid properties during the formation of calcite veins (Dietzel et al., 2009; Zheng, 2011; Azomani et al., 2013; Hou et al., 2016; Yang et al., 2018; Deininger et al., 2021). The oxygen isotope test analysis in this study shows that there is significant differentiation in oxygen isotopes, with more negative values observed in the process of strong recrystallization from micritic calcite to medium-coarse calcite veins. This suggests that these veins experienced different burial depths and had different sources of fluids during their formation. Oxygen isotope values of the powder-fine crystal veins are relatively small, and the veins are lenticular and contain pyrite. This indicates that most of these veins formed in situ at shallow burial depths, and the strength of rock-water interaction was weak. On the other hand, the more negative oxygen isotope values in medium-coarse grain veins suggest that these veins may have formed at higher temperatures and underwent long periods of rock-water interaction, fluid migration, and convergence.

Micro-zone element analysis further supports these findings, as it shows that sparry veins have a higher Mn content compared to granular veins. This suggests that interlayer water released during clay transformation was added during the later stage of vein

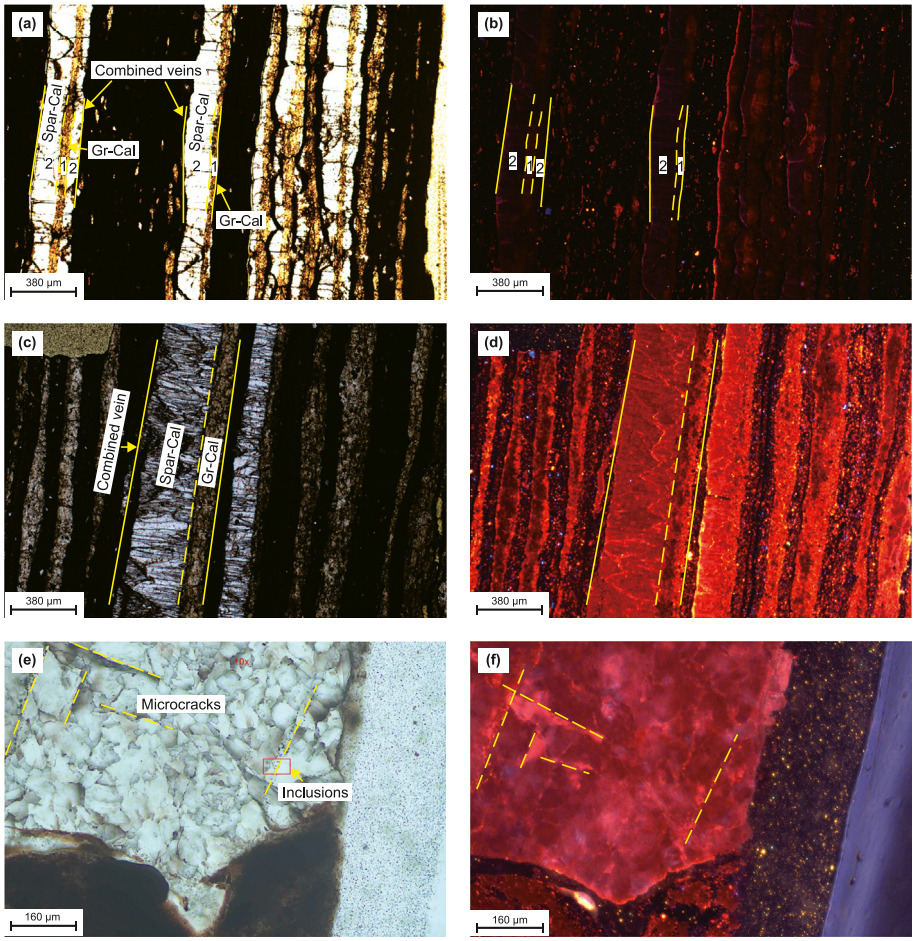

Fig. 7. Cathodoluminescence characteristics of different calcite veins. **(a)** Spar-Cal and Gr-Cal combine veins. Well N55-X1, 3334.65 m. **(b)** The figure is a CL image of **(a)**. Gr-Cal in the middle and Spar-Cal on both sides are significantly different under CL. Spar-Cal is dark purple-red, while Gr-Cal is dark red, similar to the color of micrite calcite in the surrounding rock. **(c)** Spar-Cal and Gr-Cal combine veins. Well N55-X1, 3590.17 m. **(d)** The figure is a CL image of **(c)**. The Gr-Cal veins are characterized by the combination of non-luminescent and dark-red regions, while Spar-Cal veins are dark-red or bright-red, with obvious boundaries. **(e)** Microcracks and inclusions develops in Spar-Cal vein. Well N55-X1, 3590.17 m. **(f)** The figure is a CL image of **(e)**. There are microcracks in the veins showing bright red color, which are different from veins.

formation. The presence of interlayer water accompanied by hydrocarbons significantly changed the chemical properties of the fluid (Fig. 12).

Indeed, combining the carbon and oxygen isotope analysis along with micro-element analysis provides valuable insights into the veining process in the shale. The results suggest that during the formation of calcite veins, authigenic micrite carbonate in the shale was dissolved, and various fluids with different compositions were introduced into the system, leading to changes in fluid properties. The addition of H_2S-containing fluids likely played a role in altering the fluid composition. This resulted in the development of pyrite in granular calcite veins, indicating the presence of sulfide-rich fluids during their formation. On the other hand, sparry calcite veins contain more hydrocarbons, suggesting the presence of hydrocarbon-rich fluids in their development. The increase in trace elements of Mn in sparry calcite veins further supports the idea of clay mineral conversion fluids increasing during the veining process.

5.2. Formation period of calcite veins

Calcite veins have started forming during the shallow burial period of shale, predominantly as granular calcite veins. As the organic matter matured and generated organic acids in the middle diagenetic period, thick sparry calcite veins were primarily developed. Notably, the veins formed earlier than the period of large-scale oil and gas migration. The vein formation has been continuous from the shallow burial period to the organic matter's mature stage, with relatively rapid crystallization rates during each period of vein formation. These multi-stage veins combine to create thick composite veins. Several shreds of evidence support this assertion.

(1) Morphological and grain differences between granular and sparry calcite veins

On thin sections, the vein morphology gradually transitions from lenticular to lamellar as we move from granular to sparry calcite veins. Additionally, the thickness of the veins tends to increase (Fig. 5(c)). Sparry calcite veins have the tendency to grow along the edges of granular calcite veins, eventually forming thick veins composed of both types (Fig. 5(d)). Regarding the grains, granular calcite veins exhibit a dirty appearance, while sparry calcite veins have clean and bright grains. Moreover, the grain size of sparry calcite veins is significantly larger than that of granular calcite veins. These observations strongly suggest that the formation period of granular calcite veins predates that of sparry calcite veins.

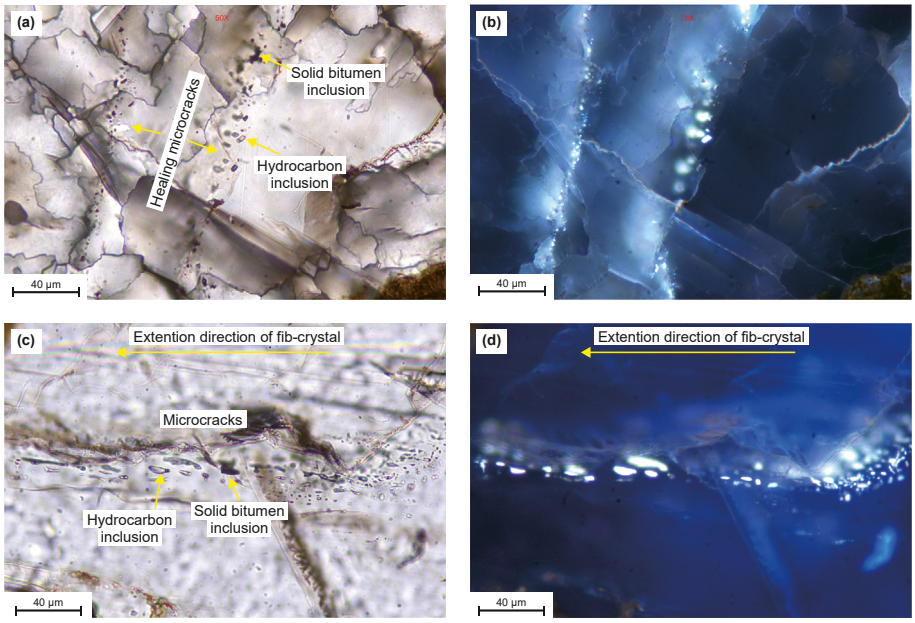

Fig. 8. Distribution of inclusions in sparry calcite veins. **(a)** On the horizontal slice, hydrocarbon inclusions and solid bitumen inclusions are beaded or banded and distributed near the healing microcracks. Well N55-X1, 3590.17 m. **(b)** The figure is a fluorescence image of **(a)**. The fluorescence color of hydrocarbon inclusions is blue white. **(c)** On the vertical slice, the inclusions are beaded and distributed near the microcracks, which is consistent with the extension direction of fibrous crystals. Well N55-X1, 3334.65 m. **(d)** The figure is a fluorescence image of **(c)**. The fluorescence color of hydrocarbon inclusions is blue white.

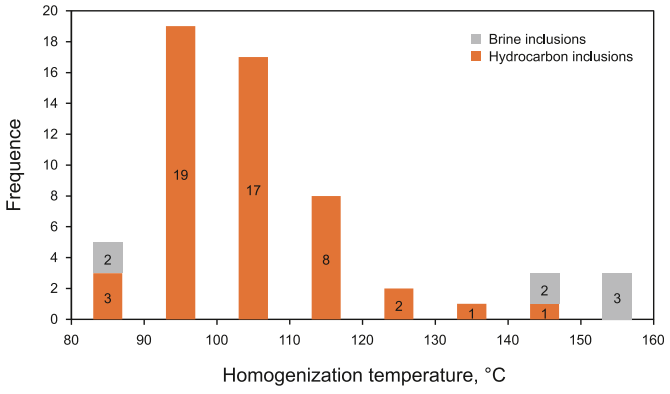

Fig. 9. Homogenization temperature characteristics of inclusions.

(2) Plastic deformation and pyrite formation in granular calcite veins

Plastic folding and deformation are evident in granular calcite veins when examining cores and thin sections. Additionally, pyrite particles larger than 10 μm are observable within these veins (Fig. 5(a), (d), (g)). The presence of plastic folding and deformation in the veins suggests that the diagenesis of shale is relatively weak, and the shale did not fully consolidate during its formation. Moreover, the occurrence of large particle-sized pyrite indicates that sulfate reduction took place during the early diagenetic stage. These two phenomena collectively imply that granular calcite veins were formed in conjunction with the crystallization of pyrite during the early stage of diagenesis.

(3) Fluorescence of sparry calcite veins

When vertically sectioned, granular calcite veins exhibit no fluorescence, while sparry calcite veins emit a distinctive blue fluorescence (Fig. 6(a)–(d)). This fluorescence pattern indicates that the formation of sparry calcite veins coincides with the generation time of oil and gas. The micro-fractures present along the lamina, which provide space for the development of calcite veins, also serve as effective conduits for oil and gas migration. Consequently, oil and gas readily enter the intercrystalline fractures and micro-fractures within sparry calcite veins.

(4) Petrography and inclusion thermometry in sparry calcite veins

Table 1
Carbon and oxygen isotope of calcite veins and surrounding rocks.

Types (sample numbers)	$\delta^{13}C_{V\text{-}PDB}$, ‰			$\delta^{18}O_{V\text{-}PDB}$, ‰		
	Minimum value	Maximum value	Average value	Minimum value	Maximum value	Average value
Micrite calcite (68)	2.28	7.91	4.13	−9.89	−2.45	−7.82
Powder-fine calcite (26)	2.24	4.9	3.72	−12.97	−7.33	−9.29
Medium calcite (22)	2.06	5.45	4	−14.12	−9.42	−11.66
Coarse calcite (18)	2.52	5.99	4.77	−13.29	−8.2	−11.38

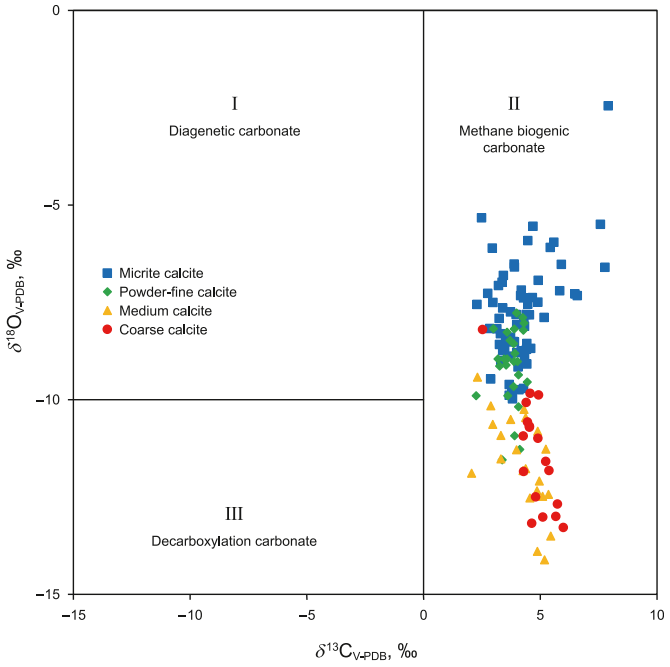

Fig. 10. Characteristics of carbon and oxygen isotope between veins in different grain sizes.

The sparry calcite veins exhibit a significant presence of two-phase hydrocarbon inclusions, and the type and distribution characteristics of these inclusions play a pivotal role in characterizing the minerals' crystallization stage and features (Li et al., 2023; Lu et al., 2023). The abundance of hydrocarbon inclusions within the veins strongly indicates their close association with the generation and migration of oil and gas. The hydrocarbon inclusions thermometry in the veins reveal a range from 80 °C to 140 °C, with the majority concentrated at 90–120 °C (Fig. 9). These temperature ranges correspond to the early to middle maturity stage of organic matter.

The inclusions analyzed in this study predominantly exhibit a distribution pattern surrounding the healing suture, appearing as beads and bands, rather than being banded along the calcite crystals (Fig. 8(a)–(d)). This observation suggests that the majority of hydrocarbon fluid inclusions were formed concurrently with the healing process of micro-cracks in the calcite crystals. Interestingly, despite the formation of the veins, the wider trapping temperature range indicates that micro-fractures continued to reform within the veins. This phenomenon highlights that, during the middle diagenetic period, the formation of sparry calcite veins occurred earlier than the time of significant oil and gas migration. Moreover, the various micro-cracks present within the calcite veins served as crucial channels for the migration of oil and gas within the veins.

(5) Differences in carbon and oxygen isotopes, cathodoluminescence, and microelements in two types of veins

Previous analyses of carbon and oxygen isotopes in calcite veins with varying grain sizes have revealed continuous fractionation of oxygen isotopes. Cathodoluminescence (CL) investigations show distinct color variations in veins from different periods. Granular calcite veins predominantly exhibit dark red coloration, whereas sparry calcite veins showcase bright red, dark red, purple, and other colors. Notably, the color of an individual vein tends to remain consistent. Furthermore, CL examination of vein combinations indicates that late veins progressively expand and widen, enveloping one or both sides of the edges of early veins and effectively filling early microcracks (Fig. 7(b), (d), (f)).

The difference in Fe and Mn element content accounts for the variation in cathodoluminescence (CL) colors between granular and sparry calcite veins. Granular calcite veins are characterized by a higher Fe content, lower Mn content, and the presence of Si and Al elements. Mn is easily oxidized to 'Mn^{4+}' and precipitates in oxidation-rich environments. The vein's characteristics, such as formation in a relatively open shallow burial environment with few clay minerals and weak recrystallization, suggest an early diagenetic period for its formation.

In contrast, sparry calcite veins exhibit a relatively higher Mn and Fe content but lower Al and Si content. The enrichment of Mn elements is attributed to organic acids produced during hydrocarbon expulsion, facilitating the extraction and accumulation of Mn. Additionally, the transformation of clay minerals contributes to the increased availability of Mn ions. The presence of relatively large negative oxygen isotope values indicates an extended period of recrystallization during its formation, aligning with the mature organic matter generation and expulsion period.

5.3. Formation process and mechanism of veins

5.3.1. Formation process

The formation process of sparry calcite veins is characterized by ctenoid texture crystals with relatively flat crystal boundaries and no apparent growth competition (Bons and Montenari, 2005; Wang et al., 2020; Su et al., 2022). Fibrous crystals on both sides of the median zone exhibit optical continuity and a symmetric change in Mn content, indicating growth along the median zone in opposite directions. In contrast, granular calcite veins lack ctenoid texture crystals, with smaller grain sizes, and often appear lenticular or thin-layered. Cathodeluminescence (CL) and electron probe microanalysis (EPMA) reveal significant differences in color and Mn content between early and late veins, but there is uniformity within a single vein. Thick asymmetric veins can result from the combination of early granular calcite veins and late sparry calcite veins or through multi-stage crystallization of sparry calcite veins, reflecting the potential influence of multi-stage fluids (Wang et al., 2023). The consistent color of a single-stage vein suggests rapid crystallization of the calcite vein. Common healing cracks are observed in the vein

Table 2
Micro-zone elements characteristics of calcite veins.

Types of vein	Content of chemical components, average/w.t.%										
	SrO	MgO	Al_2O_3	SiO_2	K_2O	CaO	TiO_2	FeO	MnO	Cr_2O_3	Total
Granular calcite veins (in lenticular, powder grain) (3)	0.628	0.259	0.664	10.681	0.071	42.327	0.006	0.752	0.005	0.021	55.413
Granular calcite veins (in thin lamellar, fine grain) (11)	0.667	0.197	0.439	4.890	0.020	47.430	0.009	0.535	0.017	0.015	54.219
Sparry calcite veins (in lamellar, medium grain) (10)	0.649	0.203	0.119	0.687	0.021	49.634	0.016	0.650	0.033	0.022	52.034
Sparry calcite veins (in lamellar, coarse grain) (26)	0.658	0.288	0.065	0.612	0.014	49.646	0.049	0.629	0.058	0.011	52.031

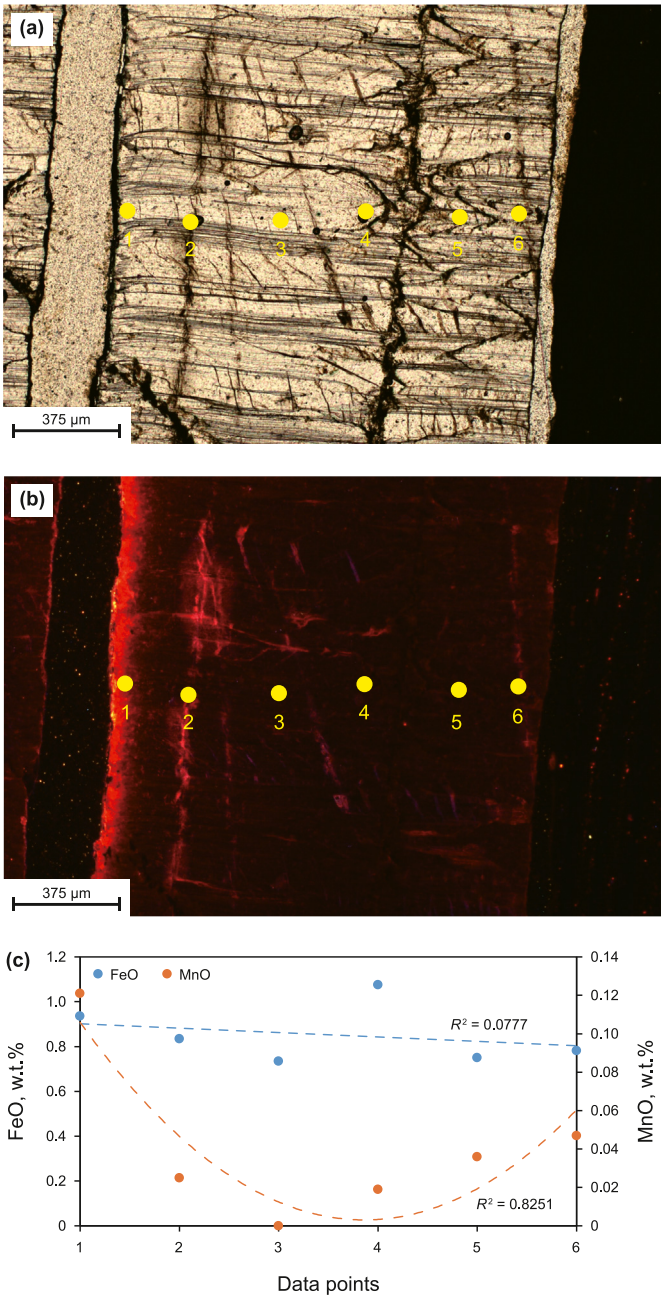

Fig. 11. Changes of FeO and MnO contents with the growth of veins. **(a)** The data point position. Well N55-X1, 3345.77 m. **(b)** The figure is a CL image of **(a)**. **(c)** Contents of FeO and MnO from edge to the midline to another edge.

body, exhibiting different CL colors from the vein body, indicating possible fracturing due to later fluid overpressure and subsequent modification of the vein's composition and structure.

The dissolved and recrystallized in situ calcite veins initially appear as fine lenticular structures, exhibiting a basic discontinuity and mainly composed of powder-fine grains. As diagenetic fluids migrate and converge over extended distances, these small lenticular veins gradually aggregate, giving rise to laminar calcite veins characterized by larger crystals and improved continuity. Evidence obtained from the carbon and oxygen isotopes of both the veins and surrounding rocks supports this interpretation (Fig. 13). The figure illustrates a lack of significant correlation between the differential value of carbon isotopes and vein thickness. Consequently, the

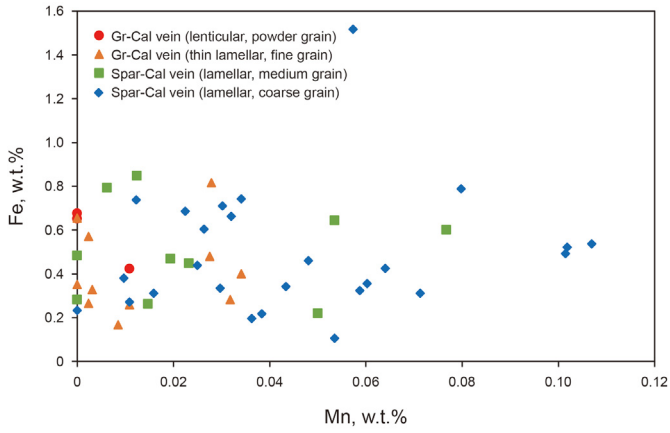

Fig. 12. The variation of Fe and Mn contents between different veins.

material source of the thick veins still originates from the shale itself, with no contribution from external substances. In contrast, as the calcite veins become thicker, a positive correlation in oxygen isotopes between the veins and surrounding rocks is observed. This phenomenon can be attributed to stronger recrystallization occurring within thicker veins due to the accumulation of diagenetic fluids from a distant source, leading to greater oxygen isotope fractionation. The oxygen isotope values of thin veins, especially lenticular veins, do not deviate significantly from those of the surrounding rocks. This finding strongly indicates that the majority of these veins are formed through in situ dissolution and precipitation processes.

Exactly, the evidence gathered from various analyses and observations suggests that the formation process of calcite veins involves continuous migration, convergence, and crystallization of diagenetic fluids along micro-fractures. As fluid overpressure plays a role, the vein-forming fluid travels further along the fracture, resulting in more significant convergence and leading to the formation of thicker veins. The presence of multi-stage fluid migration and convergence contributes to the formation of composite veins, where different stages of vein development combine to create thicker and more complex structures.

5.4. Formation mechanism

This study proposes that the formation of lamellar calcite veins exhibits long-term persistence, but the characteristics and conditions differ between the shallow burial period and the organic matter mature period.

The determination of vein formation time involves petrographic observation, inclusion thermometry, and consideration of burial and thermal history. During the shallow burial period (0–300 m, Fig. 14), sulfate bacteria utilize sulfate and organic matter, leading to the production of hydrogen sulfide and carbon dioxide, resulting in the generation of acidic water within the pores. This acidic water dissolves the calcite initially deposited in the lacustrine shale. The rapid deposition of sediments on under-compacted shales may cause overpressure in the shales (Gaarenstroom et al., 1993; Potter et al., 2005; Leynaud et al., 2007). Under the influence of compaction fluid pressure, fractures are more prone to forming along the direction of shale laminae, and carbonate-rich fluids can fill these fractured spaces. As sulfate is consumed gradually, the acidic environment changes, and the dissolved carbonate in the fractures undergoes recrystallization, resulting in the formation of calcite veins. At this early stage, the primary driving force for the formation of fractures is the abnormal high pressure generated

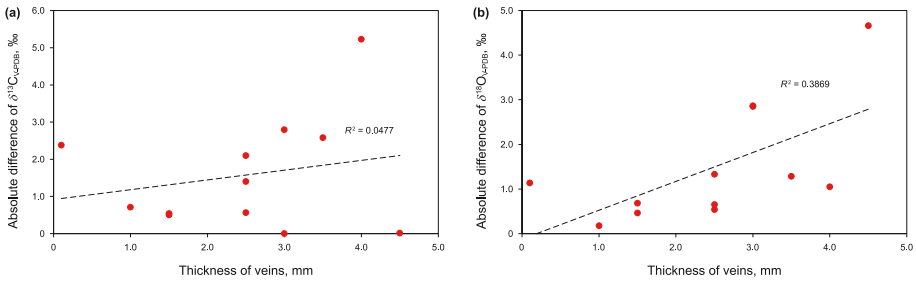

Fig. 13. The relationship of the thickness of veins and $\delta^{13}C_{V\text{-}PDB}$ **(a)** and $\delta^{18}O_{V\text{-}PDB}$ **(b)** differential value between veins and surrounding rocks.

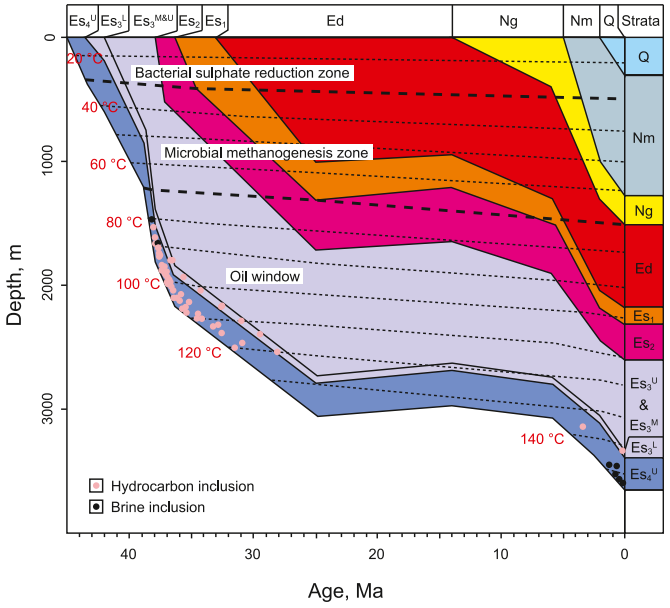

Fig. 14. Burial and thermal history of Niuzhuang Sag, Dongying Depression (modified according to reference Zhang et al., 2017).

during the under-compaction process. The distribution of veins during this period is uneven, and the generation of fluid containing hydrogen sulfide is relatively limited. Consequently, this stage is characterized by the in-situ formation of granular calcite veins containing pyrite.

As the burial depth increases (300–1200 m, Fig. 14), the dominance of methane bacteria in gas generation leads to the production of large amounts of methane and carbon dioxide. The increased carbon dioxide saturation results in a gradual cessation of the formation of early veins. With continued burial depth increase, at the late stage of early diagenesis, when the formation temperature exceeds 70 °C, the activity of methanobacteria in decomposing organic matter to generate gas essentially stops.

As the organic matter enters the mature stage and starts expelling hydrocarbons (1500–2600 m, Fig. 14), the thermal evolution of kerogen releases a significant amount of organic acids and more CO_2. This process considerably lowers the pH value of the formation water, leading to the dissolution of a large quantity of micritic carbonate minerals present in the shale laminae. Simultaneously, interlayer water released from the conversion of clay minerals provides fluids and contributes to overpressure (Bolås et al., 2004; Lahann and Swarbrick, 2011; Luan et al., 2016; Wang et al., 2018a; Zhang et al., 2020; Yu et al., 2022b). These two processes generate diagenetic fluids rich in carbonates and hydrocarbons. The overpressure resulting from hydrocarbon generation reopens fractures along the laminae and drives the migration and convergence of diagenetic fluids along the laminae direction. Upon pressure release, the carbonate-supersaturated fluids precipitate and crystallize, leading to the formation of lamellar sparry calcite veins. The abundance of fluid supply and continuous overpressure at this stage drive the fluids to migrate over long distances. Consequently, continuous migration and fluid convergence eventually culminate in the formation of thick veins. The characteristics of multi-stage veins further validate the episodic nature of hydrocarbon expulsion during thermal evolution. Even under a depth of 3000 m, the veins can still be modified by fluid activity.

Based on the above discussion, it can be inferred that during the shallow burial period, two crucial conditions contribute to the formation of fluid and micro-fractures. Firstly, the reduction of sulfate bacteria results in the generation of hydrogen sulfide and carbon dioxide, creating acidic water that dissolves the originally deposited calcite in the lacustrine shale. Secondly, the under-compaction of shale leads to overpressure, making the shale more susceptible to fracturing along the direction of shale laminae. These factors collectively promote the formation of fluid and micro-fractures during this period. As the organic matter reaches maturity, important conditions for forming fluid and microcracks shift. Organic acid expulsion, clay mineral conversion, and overpressure associated with the thermal evolution of organic matter become prominent factors. The thermal evolution of kerogen generates a substantial amount of organic acids, lowering the pH value of the formation water and facilitating the dissolution of micritic carbonate minerals within the shale laminae. The conversion of clay minerals also releases interlayer water, contributing to overpressure. Together, these processes generate diagenetic fluids rich in carbonates and hydrocarbons, which play a significant role in the formation of fluid and microcracks at this stage. The formation of calcite veins is a consequence of fluids converging and migrating along the fractures within the bedding layer due to the influence of overpressure. Micro-cracks along the laminae direction serve as crucial spaces for the crystal growth of calcite veins, and overpressure maintains the opening of these cracks, facilitating the migration of diagenetic fluids along the laminae microcracks. Under overpressure, episodic migration of diagenetic fluids along laminae microcracks, coupled with the irregular crystallization of calcite, leads to the development of multi-stage veins.

6. Conclusions

This paper focuses on investigating the material source, formation period, formation mechanism, and process of lamellar calcite veins, which are closely associated with the burial process of shale. These veins serve as crucial indicators for studying the diagenetic evolution and organic matter transformation within shale.

The study identifies two distinct types of veins with evident

petrographic differences: granular calcite veins and sparry calcite veins. These veins provide valuable records of the diagenetic history of shale during the shallow burial period and the organic matter maturity period, respectively. The material source of both types of veins is authigenic calcite present in the shale itself.

During the shallow burial period, the reduction of sulfate bacteria significantly influences the vein formation process. Concurrently, the undercompaction of shale leads to the development of overpressure, which plays a key role in promoting the formation of granular calcite veins. As the burial depth increases, the influence of sulfate bacteria weakens, while the hydrocarbon expulsion of organic matter commences. The dissolution of organic acids and the overpressure generated during the process of hydrocarbon generation are important factors driving the formation of sparry calcite veins.

The formation of veins is a complex process involving continuous migration, convergence, and crystallization of vein-forming fluid. Initially, lenticular veins are formed through near-in-situ convergence of fluid. However, as the fluid continues to converge along fractures and migrates over longer distances, the veins undergo a transformation, becoming laminated with increased thickness. The formation of veins occurs in multiple stages, and a vein may be the result of rapid crystallization or a multi-stage crystallization process. Composite veins can arise from a combination of early and late veins or through multi-stage crystallization of late veins. After the formation, veins may undergo modifications due to the influence of later fluids. The formation of composite veins and the modification of veins indicate the occurrence of multi-stage fluid activities and fluid evolution during the diagenetic evolution of shale.

Declaration of competing interest

The authors declare that they have no known competing financial interests or personal relationships that could have appeared to influence the work reported in this paper.

Acknowledgement

This paper acknowledges the support of the National Natural Science Foundation of China (project number: 41572123). The authors express their gratitude to the Geology Institute of SINOPEC Shengli Oilfield for providing the test samples. The experimental testing of samples was conducted with the assistance of China University of Petroleum (East China) and Ocean University of China, for which the authors extend their appreciation.

References

Al-Aasm, I.S., Muir, I., Morad, S., 1993. Diagenetic conditions of fibrous calcite vein formation in black shales: petrographic, chemical and isotopic evidence. Bull. Can. Petrol. Geol. 41, 46–56. https://doi.org/10.35767/gscpgbull.41.1.046.

Al-Aasm, I.S., Coniglio, M., Desrochers, A., 1995. Formation of complex fibrous calcite veins in upper triassic strata of wrangellia terrain, British columbia, Canada. Sediment. Geol. 100, 83–95. https://doi.org/10.1016/0037-0738(95)00104-2.

Azomani, E., Azmy, K., Blamey, N., Brand, U., Al-Aasm, I.S., 2013. Origin of Lower Ordovician dolomites in eastern Laurentia: controls on porosity and implications from geochemistry. Mar. Petrol. Geol. 40, 99–114. https://doi.org/10.1016/j.marpetgeo.2012.10.007.

Bolås, H.M.N., Hermanrud, C., Teige, G.M.G., 2004. Origin of overpressures in shales: constraints from basin modeling. Am. Assoc. Petrol. Geol. Bull. 88, 193–211. https://doi.org/10.1306/10060302042.

Bons, P.D., Montenari, M., 2005. The formation of antitaxial calcite veins with well-developed fibres, Oppaminda Creek, South Australia. J. Struct. Geol. 27, 231–248. https://doi.org/10.1016/j.jsg.2004.08.009.

Bons, P.D., Elburg, M.A., Gomez-Rivas, E., 2012. A review of the formation of tectonic veins and their microstructures. J. Struct. Geol. 43, 33–62. https://doi.org/10.1016/j.jsg.2012.07.005.

Cobbold, P.R., Rodrigues, N., 2007. Seepage forces, important factors in the formation of horizontal hydraulic fractures and bedding-parallel fibrous veins ('beef'and 'cone-in-cone'). Geofluids 7 (3), 313–322. https://doi.org/10.1111/j.1468-8123.2007.00183.x.

Cobbold, P.R., Zanella, A., Rodrigues, N., Løseth, H., 2013. Bedding-parallel fibrous veins (beef and cone-in-cone): worldwide occurrence and possible significance in terms of fluid overpressure, hydrocarbon generation and mineralization. Mar. Petrol. Geol. 43, 1–20. https://doi.org/10.1016/j.marpetgeo.2013.01.010.

Cao, Z., Lin, C.Y., Dong, C.M., Ren, L.H., Han, S., Dai, J.J., Xu, X., Qin, M.Y., Zhu, P., 2018. Impact of sequence stratigraphy, depositional facies, diagenesis and CO_2 charge on reservoir quality of the lower cretaceous Quantou Formation. Southern Songliao Basin, China. Mar. Petrol. Geol. 93, 497–519. https://doi.org/10.1016/j.marpetgeo.2018.03.015.

Chen, Z.H., Jiang, W.B., Zhang, L.Y., Zha, M., 2018. Organic matter, mineral composition, pore size, and gas sorption capacity of lacustrine mudstones: implications for the shale oil and gas exploration in the Dongying Depression, eastern China. AAPG (Am. Assoc. Pet. Geol.) Bull. 102 (8), 1565–1600. https://doi.org/10.1306/0926171423117184.

Durney, D.W., Ramsay, J.G., 1973. Incremental strain measured by syntectonic crystal growths. In: De Jong, K.A., Scholten, R. (Eds.), Gravity and Tectonics. John Wiley & Sons, New York, pp. 67–96.

Dietzel, M., Tang, J.W., Leis, A., Köhler, S.J., 2009. Oxygen isotopic fractionation during inorganic calcite precipitation—Effects of temperature, precipitation rate and pH. Chem. Geol. 268 (1–2), 107–115. https://doi.org/10.1016/j.chemgeo.2009.07.015.

Deininger, M., Hansen, M., Fohlmeister, J., Schröder-Ritzrau, A., Burstyn, Y., Scholz, D., 2021. Are oxygen isotope fractionation factors between calcite and water derived from speleothems systematically biased due to prior calcite precipitation (PCP)? Geochem. Cosmochim. Acta 305, 212–227. https://doi.org/10.1016/j.gca.2021.03.026.

Gaarenstroom, L., Tromp, R., Brandenburg, A., 1993. Overpressures in the Central North Sea: implications for trap integrity and drilling safety. In: Parker, J.R. (Ed.), Petroleum Geology of Northwest Europe. Proceedings of the 4th Conference. Geological Society, London, pp. 1305–1313. https://doi.org/10.1144/0041305.

Gallagher, K.L., Dupraz, C., Visscher, P.T., 2014. Two opposing effects of sulfate reduction on carbonate precipitation in normal marine, hypersaline, and alkaline environments: comment. Geology 42, 313–314. https://doi.org/10.1130/G34639C.1.

Hou, Y., Azmy, K., Berra, F., Jadoul, F., Blamey, N.J.F., Gleeson, S.A., Brand, U., 2016. Origin of the Breno and Esino dolomites in the western southern Alps (Italy): implications for a volcanic influence. Mar. Petrol. Geol. 69, 38–52. https://doi.org/10.1016/j.marpetgeo.2015.10.010.

Hrabovszki, E., Tóth, E., Tóth, T.M., Máthé, Z., Schubert, F., 2020. Potential formation mechanisms of early diagenetic displacive veins in the Permian Boda Claystone Formation. J. Struct. Geol. 138, 104098. https://doi.org/10.1016/j.jsg.2020.104098.

Irwin, H., Curtis, C., Coleman, M., 1977. Isotopic evidence for source of diagenetic carbonates formed during burial of organic-rich sediments. Nature 269 (5625), 209–213. https://doi.org/10.1038/269209a0.

Lahann, R.W., Swarbrick, R.E., 2011. Overpressure generation by load transfer following shale framework weakening due to smectite diagenesis. Geofluids 11, 362–375. https://doi.org/10.1111/j.1468-8123.2011.00350.x.

Lang, W.D., Spath, L.F., Richardson, W.A., 1923. Shales with 'beef', a sequence in the lower lias of the dorset coast. Q. J. Geol. Soc. Lond. 79, 47–66. https://doi.org/10.1144/GSL.JGS.1923.079.01-04.05.

Larmier, S., Zanella, A., Lejay, A., Mourgues, R., Gelin, F., 2021. Geological parameters controlling the beddingparallel vein distribution in Vaca Muerta Formation core data, Neuquén Basin, Argentina. AAPG (Am. Assoc. Pet. Geol.) Bull. 105 (11), 2221–2243. https://doi.org/10.1306/03122119201.

Leynaud, D., Sultan, N., Mienert, J., 2007. The role of sedimentation rate and permeability in the slope stability of the formerly glaciated Norwegian continental margin: the Storegga slide model. Landslides 4, 297–309. https://doi.org/10.1007/s10346-007-0086-z.

Liang, C., Cao, Y.C., Liu, K.Y., Jiang, Z.X., Wu, J., Hao, F., 2018. Diagenetic variation at the lamina scale in lacustrine organic-rich shales: implications for hydrocarbon migration and accumulation. Geochem. Cosmochim. Acta 229, 112–128. https://doi.org/10.1016/j.gca.2018.03.017.

Li, Z.X., Yang, W., Wang, Y.S., Zhang, L.Q., Luo, H.M., Liu, S.H., Zhang, L.K., Luo, X.R., 2019. Anatomy of a lacustrine stratigraphic sequence within the fourth member of the Eocene Shahejie Formation along the steep margin of the Dongying Depression, eastern China. AAPG (Am. Assoc. Pet. Geol.) Bull. 103 (2), 469–504. https://doi.org/10.1306/08031817307.

Liu, H.M., Zhang, S., Song, G.Q., Wang, X.J., Teng, J.B., Wang, M., Bao, Y.S., Yao, S.P., Wang, W.Q., Zhang, S.P., Hu, Q.H., Fang, Z.W., 2019. Effect of shale diagenesis on pores and storage capacity in the Paleogene Shahejie Formation, dongying depression, Bohai Bay Basin, east China. Mar. Petrol. Geol. 103, 738–752. https://doi.org/10.1016/j.marpetgeo.2019.01.002.

Lu, K., Huang, Y.H., He, S., X, Y.H., M, J.H., F, D.Y., W, Z.R., 2023. Indication of geochemical indexes for shale gas preservation conditions in shale fractures vein : evidence from Yangzi Permian organic-rich shale in the Leping Formation. Nat. Gas Geosci. 34 (6), 1090–1102. https://doi.org/10.11764/j.issn.1672-1926.2023.03.008 (in Chinese).

Luan, G.Q., Dong, C.M., Ma, C.F., Lin, C.Y., Zhang, J.Y., Lu, X.F., 2016. Pyrolysis simulation experiment study on diagenesis and evolution of organic-rich shale. Acta Sedimentol. Sin. 34 (6), 1208–1216. https://doi.org/10.14027/j.cnki.cjxb.2016.06.018 (in Chinese).

Luan, G.Q., Dong, C.M., Azmy, K., Lin, C.Y., Ma, C.F., Ren, L.H., Zhu, Z.C., 2019. Origin of bedding-parallel fibrous calcite veins in lacustrine black shale: a case study from Dongying Depression, Bohai Bay Basin. Mar. Petrol. Geol. 102, 873–885. https://doi.org/10.1016/j.marpetgeo.2019.01.010.

Li, Q., You, X., Jiang, Z.X., Wu, S.H., Zhang, R.F., 2020. The origins of carbonate minerals of a source-controlled lacustrine carbonate succession in the Shulu sag, Bohai Bay Basin: implications for porosity development and paleoenvironment. Mar. Petrol. Geol. 122, 104673. https://doi.org/10.1016/j.marpetgeo.2020.104673.

Li, X.J., Li, F., Deng, S.L., Wu, J., Deng, B., Liu, S.G., 2023. Vein-forming fluid characteristics and implications of fluid activity for shale gas preservation of Qiongzhusi Formation at Micangshan front in northern Sichuan, 2023 Pet. Geol. Oilfield Dev. Daqing 42 (5), 27–35. https://doi.org/10.19597/J.ISSN.1000-3754.202210063. No.219 (in Chinese).

Ma, C.F., Dong, C.M., Luan, G.Q., Lin, C.Y., Liu, X.C., Elsworth, D., 2016. Types, characteristics and effects of natural fluid pressure fractures in shale: a case study of the Paleogene strata in Eastern China. Petrol. Explor. Dev. 43 (4), 634–643. https://doi.org/10.1016/S1876-3804(16)30074-X.

Ma, C.F., Dong, C.M., Elsworth, D., Wang, Q., 2020. Insights from electron backscatter diffraction into the origin of fibrous calcite veins in organic-rich shale from lower Es3 to upper Es4, Jiyang Depression, China. Mar. Petrol. Geol. 113, 104131. https://doi.org/10.1016/j.marpetgeo.2019.104131.

Mack, G.H., Cole, D.R., Giordano, T.H., Schaal, W.C., Barcelos, J.H., 1991. Paleoclimatic controls on stable oxygen and carbon isotopes in caliche of the Abo Formation (Permian), south-central New Mexico, USA. J. Sediment. Res. 61 (4), 458–472. https://doi.org/10.1306/D426773A-2B26-11D7-8648000102C1865D.

Maher, H.D., Ogata, K., Braathen, A., 2017. Cone-in-cone and beef mineralization associated with Triassic growth basin faulting and shallow shale diagenesis, Edgeøya, Svalbard. Geol. Mag. 154, 201–216. https://doi.org/10.1017/S0016756815000886.

Means, W.D., Li, T., 2001. A laboratory simulation of fibrous veins: some first observations. J. Struct. Geol. 23 (6–7), 857–863. https://doi.org/10.1016/S0191-8141(00)00158-9.

Meng, Q.F., Hooker, J., Cartwright, J., 2017. Early overpressuring in organic-rich shales during burial: evidence from fibrous calcite veins in the Lower Jurassic Shales-with-Beef Member in the Wessex Basin, UK. J. Geol. Soc. 174 (5), 869–882. https://doi.org/10.1144/jgs2016-146.

Meng, Q.F., Hooker, J., Cartwright, J., 2018. Displacive widening of calcite veins in shale: insights into the force of crystallization. J. Sediment. Res. 88, 327–343. https://doi.org/10.2110/jsr.2018.18.

Meng, Q.F., Hooker, J., Cartwright, J., 2019. Role of pressure solution in the formation of bedding-parallel calcite veins in an immature shale (Cretaceous, southern UK). Geol. Mag. 156, 918–934. https://doi.org/10.1017/S0016756818000377.

Myrttinen, A., Becker, V., Barth, J.A.C., 2012. A review of methods used for equilibrium isotope fractionation investigations between dissolved inorganic carbon and CO_2. Earth Sci. Rev. 115 (3), 192–199. https://doi.org/10.1016/j.earscirev.2012.08.004.

Oliver, N.H.S., Bons, P.D., 2001. Mechanisms of fluid flow and fluid-rock interaction in fossil metamorphic hydrothermal systems inferred from vein-wallrock patterns, geometry and microstructure. Geofluids 1 (2), 137–162. https://doi.org/10.1046/j.1468-8123.2001.00013.x.

Pang, S.Y., Cao, Y.C., Liang, C., 2019. Lithofacies characteristics and sedimentary environment of Es4U and Es3L: a case study of Well FY1 in Dongying sag, Bohai Bay Basin. Oil Gas Geol. 40 (4), 799–809. https://doi.org/10.11743/ogg20190410 (in Chinese).

Peng, J., Xu, T.Y., Yu, L.D., 2020. Characteristics and controlling factors of lacustrine fine-grained sediments of the fourth member of Shahejie Formation in Dongying Depression. Lithologic Reservoirs 32 (5), 1–12. https://doi:10.12108/yxyqc.20200501 (in Chinese).

Potter, P.E., Maynard, J.B., Depetris, P.J., 2005. Mud and mudstones: introduction and overview. Econ. Geol. 100 (7), 1469–1471. https://doi.org/10.2113/gsecongeo.100.7.1469.

Raiswell, R., 1987. Non-steady state microbiological diagenesis and the origin of concretions and nodular limestones. Geological Society, London, Special Publications 36 (1), 41–54. https://doi.org/10.1144/GSL.SP.1987.036.01.05.

Ramsay, J.G., 1980. The crack–seal mechanism of rock deformation. Nature 284, 135. https://doi.org/10.1038/284135a0.

Rodrigues, N.T., 2008. Fracturation hydraulique et forces decourant: modélisation analogique et données de terrain. Ph.D. thesis, Universite de Rennes, Rennes, France, p. 161.

Rodrigues, N., Cobbold, P.R., Loseth, H., Ruffet, G., 2009. Widespread bedding-parallel veins of fibrous calcite ('beef') in a mature source rock (Vaca Muerta Fm, Neuquén Basin, Argentina): evidence for overpressure and horizontal compression. J. Geol. Soc. 166 (4), 695–709. https://doi.org/10.1144/0016-76492008-111.

Stoneley, R., 1983. Fibrous calcite veins, overpressures, and primary oil migration. AAPG (Am. Assoc. Pet. Geol.) Bull. 67 (9), 1427–1428. https://doi.org/10.1306/03B5BA47-16D1-11D7-8645000102C1865D.

Su, A., Bons, P.D., Chen, H., Feng, Y.X., Zhao, J.X., Song, J.W., 2022. Age, material source, and formation mechanism of bedding-parallel calcite beef veins: case from the mature Eocene lacustrine shales in the Biyang Sag, Nanxiang Basin, China. GSA Bulletin 134 (7–8), 1811–1833. https://doi.org/10.1130/B35866.1.

Tribovillard, N., Petit, A., Quijada, M., Riboulleau, A., Sansjofre, P., Thomazo, C., Huguet, A., Birgel, D., Averbuch, O., 2018. A genetic link between synsedimentary tectonics-expelled fluids, microbial sulfate reduction and cone-in-cone structures. Mar. Petrol. Geol. 93, 437–450. https://doi.org/10.1016/j.marpetgeo.2018.03.024.

Teng, J.B., Liu, H.M., Qiu, L.W., Zhang, S.P., 2020. Sedimentary and diagenetic characteristics of lacustrine fine-grained hybrid rock in Paleogene formation in Dongying Sag. Earth Sceince 45 (10), 3808–3826. https://doi/10.3799/dqkx.2020.127.

Teng, J.B., 2020. Origin and evidence of calcite in shale oil reservoir of Dongying Sag. Petroleum Geology and Recovery Efficiency 27 (2), 18–25. https://doi:10.13673/j.cnki.cn37-1359/te.2020.02.003 (in Chinese).

Ukar, E., Lopez, R.G., Gale, J.F., Laubach, S.E., Manceda, R., 2017. New type of kinematic indicator in bedparallel veins, late jurassic–early cretaceous Vaca Muerta formation, Argentina: EW shortening during late cretaceous vein opening. J. Struct. Geol. 104, 31–47. https://doi.org/10.1016/j.jsg.2017.09.014.

Ukar, E., Lopez, R.G., Gale, J.F., Laubach, S.E., Manceda, Fall, A., Brisson, I., 2020. Natural fractures: from core and outcrop observations to subsurface models. AAPG Memoir 121, 377–416. https://doi:10.1306/13682234M1203837.

Wang, G.M., Ren, Y.J., Zhong, J.H., Ma, Z.P., Jiang, Z.X., 2005. Genetic analysis on lamellar calcite Veins in Paleogene black shale of the Jiyang Depression. Acta Geol. Sin. 79 (6), 834–838 (in Chinese).

Wang, M., Chen, Y., Song, G.Q., Matthew, S.-M., Liu, Q., Wang, X.J., Zhang, X.J., Zhao, Z.Y., Liu, W.Y., Zhang, H.J., Zhou, Z.Y., 2018a. Formation of bedding-parallel, fibrous calcite veins in laminated source rocks of the Eocene Dongying Depression: a growth model based on petrographic observations. Int. J. Coal Geol. 200, 18–35. https://doi.org/10.1016/j.coal.2018.10.004.

Wang, M., Lu, J.L., Zuo, Z.X., Li, H., Wang, B.H., 2018b. Characteristics and dominating factors of lamellar fine-grained sedimentary rocks: a case study of the upper Es4 member - lower Es3 member, Dongying Sag, Bohai Bay Basin. Petroleum Geology & Experiment 40 (4), 470–478. https://doi:10.11781/sysydz201804470.

Wang, M., Chen, Y., Bain, W.M., Song, G.Q., Liu, K.Y., Zhou, Z.Z., Matthew, S.-M., 2020. Direct evidence for fluid overpressure during hydrocarbon generation and expulsion from organic-rich shales. Geology 48, 374–378. https://doi.org/10.1130/G46650.1.

Wang, M., Chen, Y., Richard, A.S., Ashley, W., Zhou, Y.Q., Song, G.Q., Zhou, T.F., Matthew, S.-M., 2023. Fibrous calcite veins record stepwise, asymmetric opening and episodic hydrocarbon expulsion from organic-rich shales. Geology. https://doi.org/10.1130/G50792.1.

Wolff, G.A., Rukin, N., Marshall, J.D., 1992. Geochemistry of an early diagenetic concretion from the Birchi Bed (L. Lias, W. Dorset, UK). Org. Geochem. 19 (4–6), 431–444. https://doi.org/10.1016/0146-6380(92)90010-U.

Wu, J., Jiang, Z.X., Wang, X., 2018. Sequence stratigraphy characteristics of lacustrine fine-grained sedimentary rocks: a case study of the Upper fourth member of Paleogene Shahejie Formation, Dongying Sag, Bohai Bay Basin. Nat. Gas Geosci. 29 (2), 199–210. https://doi:10.11764/j.issn.1672-1926.2018.01.005 (in Chinese).

Wu, A.B., Cao, J., Zhang, J.K., 2021. Bedding-parallel calcite veins indicate hydrocarbon–water–rock interactions in the over-mature Longmaxi shales, Sichuan Basin. Mar. Petrol. Geol. 133, 105303. https://doi.org/10.1016/j.marpetgeo.2021.105303.

Yang, G.S., Wen, H.J., Hu, R.Z., Fan, L.W., Yan, Y.F., Mao, Z.B., Wang, K., 2018. Sources and evolution of the Ore-forming materials in the anqing Cu-Fe deposit in anhui province—geological and S, C, O isotopic constraints. Geotect. Metallogenia 42 (4), 651–663. https://doi:10.16539/j.ddgzyckx.2018.03.013 (in Chinese).

Yu, Z.Y., Chen, S.Y., Zhang, S., Liu, X.J., Tang, D., Yan, J.H., 2022b. Influence of diagenesis on reservoir performance of shale: a case study of the upper submember of Member 4 of Paleogene Shahejie Formation in Dongying sag. J. Palaeogeogr. 24 (4), 771–784. https://doi:10.7605/gdlxb.2022.04.046 (in Chinese).

Yu, L.D., Peng, J., Xu, T.Y., Han, H.D., Yang, Y.M., 2022a. Analysis of organic enrichment and influences in fine-grained sedimentary strata in saline lacustrine basins of continental fault depressions: case study of the upper sub-segment of the upper 4th member of the Shahejie Formation in the Dongying Depression. Acta Sedimentol. Sin. 1–31. https://doi.org/10.14027/j.issn.1000-0550.2022.096, 2023-04-01 (in Chinese).

Yu, H., Zhou, X.Q., Wang, J.G., Guo, C., Wei, H.Y., Chen, D.Z., 2015. The origin of bedding-parallel fibrous calcite veins in the lower permian Chihsia formation in western Hubei province, south China. Sci. Bull. 60 (20), 1778–1786. https://doi.org/10.1007/s11434-015-0903-z.

Zanella, A., Cobbold, P.R., Rojas, L., 2014. Beef veins and thrust detachments in Early Cretaceous source rocks, foothills of Magallanes-Austral Basin, southern Chile and Argentina: structural evidence for fluid overpressure during hydrocarbon maturation. Mar. Petrol. Geol. 55, 250–261. https://doi.org/10.1016/j.marpetgeo.2013.10.006.

Zanella, A., Cobbold, P.R., Boassen, T., 2015a. Natural hydraulic fractures in the Wessex Basin, SW England: widespread distribution, composition and history. Mar. Petrol. Geol. 68, 438–448. https://doi.org/10.1016/j.marpetgeo.2015.09.005.

Zanella, A., Cobbold, P.R., Ruffet, G., Leanza, H.A., 2015b. Geological evidence for fluid overpressure, hydraulic fracturing and strong heating during maturation and migration of hydrocarbons in Mesozoic rocks of the northern Neuquén Basin, Mendoza Province, Argentina. J. S. Am. Earth Sci. 62, 229–242. https://doi.org/10.1016/j.jsames.2015.06.006.

Zanella, A., Cobbold, P.R., Rodrigues, N., Løseth, H., Jolivet, M., Gouttefangeas, F., Chew, D., 2021. Source rocks in foreland basins: a preferential context for the development of natural hydraulic fractures. AAPG (Am. Assoc. Pet. Geol.) Bull. 105 (4), 647–668. https://doi.org/10.1306/08122018162.

Zhang, J.G., Jiang, Z.X., Jiang, X.L., Wang, S.Q., Liang, C., Wu, M.H., 2016. Oil generation induces sparry calcite formation in lacustrine mudrock, Eocene of east China. Mar. Petrol. Geol. 71, 344–359. https://doi.org/10.1016/j.marpetgeo.2016.01.007.

Zhang, J.G., Jiang, Z.X., Wang, S.Q., Wang, R.Y., Zhang, Y.F., Du, W., 2021. Bedding-parallel calcite veins as a proxy for shale reservoir quality. Mar. Petrol. Geol. 127, 104975. https://doi.org/10.1016/j.marpetgeo.2021.104975.

Zhang, P.H., Chen, Z.Y., Xue, L., Bao, Y.J., Fang, Y., 2020. The differential diagenetic evolution and its influencing factors of Lower Cambrian black rock series in the northwestern margin of Tarim Basin. Acta Petrol. Sin. 36 (11), 3463–3476. https://doi:10.18654/1000-0569/2020.11.13 (in Chinese).

Zhang, S.M., Cao, Y.C., Wang, Y.Z., Yang, T., Wang, W., Wang, J.S., 2017. Diagenesis and physical properties evolution of turbidite reservoirs in Es3z of Niuzhuang sag, Dongying Depression. Journal of China University of Petroleum (Edition of Natural Science) 41 (2), 1–11. https://doi:10.3969/j.issn.1673-5005.2017.02.001 (in Chinese).

Zhang, Z., Pang, J., Yang, Y.T., Cao, Y.H., Qi, M.H., Zhang, H.Y., Zhang, L., Ma, S., 2022. Carbon and oxygen isotope characteristics and genesis of carbonate cements in sandstone of the 4th Member of the Xujiahe Formation in the centralwestern Sichuan depression, Sichuan basin, China. Acta Geol. Sin. 96 (6), 2094–2106. https://doi:10.19762/j.cnki.dizhixuebao.2022260 (in Chinese).

Zhao, B.S., Li, R.X., Wu, X.L., Tan, X.L., Zhao, D., Liu, Q., Ahmed, K., 2020. The fibrous crystal growth driven byforce of crystallization: petrographic evidence of antiaxial fibrous gypsum veins in the Qingshuying Formation of the Ningnan Basin. Bull. China Soc. Mineral Petrol. Geochem. 39 (2), 293–303. https://doi:10.19658/j.issn.1007-2802.2020.39.002 (in Chinese).

Zhao, X.Z., Li, Q., Jiang, Z.X., Zhang, R.F., Li, H.P., 2014. Organic geochemistry and reservoir characterization of the organic matter-rich calcilutite in the Shulu sag, Bohai Bay Basin, North China. Mar. Petrol. Geol. 51, 239–255. https://doi.org/10.1016/j.marpetgeo.2013.12.014.

Zheng, Y.F., 2011. On the theoretical calculations of oxygen isotope fractionation factors for carbonate-water systems. Geochem. J. 45 (4), 341–354. https://doi.org/10.2343/geochemj.1.0125.